

High-speed three-wave polarimeter-interferometer diagnostic for Madison symmetric torus

B. H. Deng, D. L. Brower, and W. X. Ding

Electrical Engineering Department, University of California, Los Angeles, California 90095

M. D. Wyman, B. E. Chapman, and J. S. Sarff

Department of Physics, University of Wisconsin, Madison, Wisconsin 53706

(Received 5 May 2006; presented on 10 May 2006; accepted 11 June 2006; published online 27 September 2006)

A high-speed three-wave polarimeter-interferometer diagnostic has been developed on the Madison symmetric torus reversed field pinch to provide simultaneous measurement of electron density and poloidal magnetic field profile evolution. With increased digitizer bandwidth, polarimetry noise due to aliasing and cross-talk is minimized, and time response improved. System performance is demonstrated by measurements of equilibrium profile evolution during fast events such as the sawtooth crash and pellet injection. © 2006 American Institute of Physics.

[DOI: [10.1063/1.2222332](https://doi.org/10.1063/1.2222332)]

I. INTRODUCTION

Far infrared (FIR) laser interferometry and polarimetry have been successfully used to diagnose reversed field pinch plasmas in the Madison symmetric torus (MST). Equilibrium and fluctuating quantities of plasma electron density, magnetic field, and current density have been measured.¹⁻³ In these experiments, the FIR laser system was operated as either a multi-channel interferometer or a polarimeter diagnostic, separately. To reconstruct the equilibrium current and magnetic field profiles and to extract the fluctuation information, it was necessary to have sets of ensemble-averaged data from each measurement. In plasma discharges that vary from shot to shot, such as in pellet injection experiments or high confinement plasmas, simultaneous interferometer and polarimeter measurements are necessary to accurately assess plasma performance. This has been achieved by adding a third FIR laser to the system, making a three-wave polarimeter-interferometer. Initial results from this new diagnostic system under various plasma conditions are presented along with a description of the analysis technique.

II. THREE-WAVE POLARIMETER-INTERFEROMETER DIAGNOSTIC SYSTEM

The three-wave polarimeter-interferometer diagnostic, shown schematically in Fig. 1, has previously been described in detail.^{2,4} About 100 W of CO₂ laser output power is subdivided to pump three FIR lasers filled with formic acid (HCOOH) vapor. A maximum power of ~20 mW is obtained from each cavity at wavelength $\lambda_0=432 \mu\text{m}$ and is sufficient for 11-channel operation. Laser beams from FIR cavities 1 and 2 (see Fig. 1) are made collinear and converted into right-hand and left-hand circularly polarized beams using a polarizer and quarter-wave plate. The combined beams are then subdivided into a reference beam and 11 discrete probe beams. For clarity, only 1 of the 11 probe beams is shown in Fig. 1. The third FIR laser beam is routed to the

mixers and used as local oscillator drive. FIR 2 laser cavity is tuned to produce maximum output power, while FIR 1 and 3 laser cavities are slightly detuned to produce intermediate frequency (IF) signals.

The IF signals from each mixer are directly digitized and stored in the database. Shown in Fig. 2 is a typical IF signal power spectrum obtained during a plasma discharge. The IF signal peaking at ~0.73 MHz is the beat signal between FIR lasers 1 and 2 and carries the Faraday rotation information; the IF signals peaking at ~1.17 and ~1.9 MHz are the beat signals between FIR lasers 2 and 3, and 1 and 3, respectively, and carry the interferometer phase for the *R* and *L* waves. In addition to these three main IF peaks, there are secondary peaks resulting from self-mixing between the three main bands. For example, the small peak at ~1.46 MHz is the second harmonic of the polarimetry carrier at 0.73 MHz, and the peak at ~2.93 MHz is the aliased (for 6 MHz sampling rate) sum frequency of the two interferometry carriers. Although these secondary peaks are more than 30 dB weaker than the main polarimetry and interferometry carriers, they are comparable in amplitude to the high frequency Faraday rotation and electron density fluctuations which appear as a broadening of the main carrier frequencies. If not properly arranged, the secondary peaks can fall into the main IF detection bands (boxes shown in Fig. 2) and effectively increase the system noise level. For a given digitizer bandwidth, there is an optimum IF arrangement that provides maximum separation of the secondary peaks from the main IF peaks, and, therefore, maximum detection bandwidth. For digitizer sampling speed of 6 MHz, the optimum IFs are ~0.7, ~1.1, and 1.8 MHz, which provide bandwidths of ~100 kHz for polarimetry and >200 kHz for interferometry measurements, as shown by the boxes in Fig. 2. The separation between the polarimetry carrier and the lower frequency interferometry carrier is ~400 kHz; therefore, the cross-talk between polarimetry and interferometry due to broadband plasma fluctuations is negligible. The Nyquist frequency of

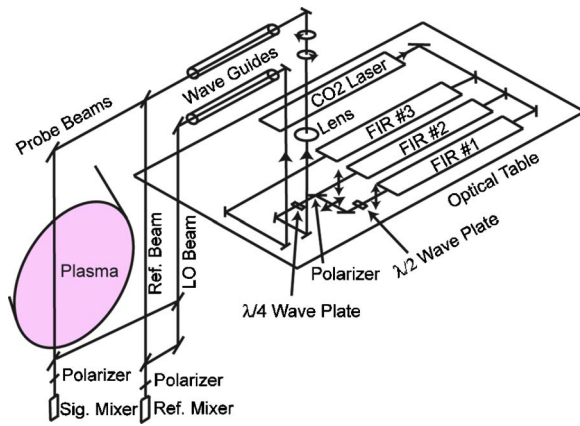


FIG. 1. (Color online) Schematic diagram of the three-wave polarimeter-interferometer for MST. The impact parameters of the 11 probe beams are -32 , -24 , -17 , -9 , -2 , 6 , 13 , 21 , 28 , 36 , and 43 cm, respectively. For clarity, only one probe beam is shown.

3 MHz is close to the amplifier bandwidth, which serves to minimize aliasing of high frequency broadband noise into the detection bands. These bandwidth limits give excellent results for equilibrium and fluctuation measurements in MST.

A digital phase comparator technique⁵ is applied to the stored signals from the 11 chords and reference in order to extract the time series data of Faraday rotation and line-integrated density. Simultaneous multichord density and Faraday rotation data for a standard 400 kA discharge in MST are shown in Fig. 3. All time series traces are low-pass filtered at 50 kHz and plotted every $10 \mu\text{s}$. The sawtooth oscillations are clearly shown in both the interferometry and polarimetry data. Higher frequency oscillations are due to plasma fluctuations. Maximum Faraday rotation angles measured are $\sim 4^\circ$ and change sign when going across the magnetic axis, as expected. In addition, the chord with impact parameter nearest the magnetic axis, $x=6$ cm, shows a phase change near zero, consistent with no equilibrium magnetic field being aligned along the laser beam.

III. DATA ANALYSIS AND EXPERIMENTAL RESULTS

Electron density profiles are obtained directly from the 11-chord interferometer data via inversion.^{2,6} Subsequently, a

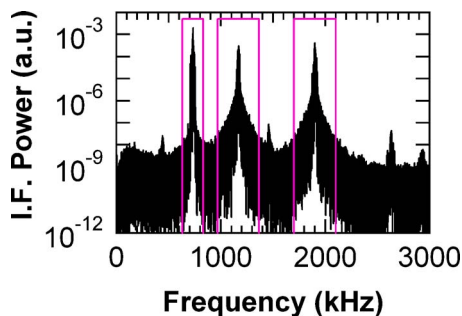


FIG. 2. (Color online) Typical probe signal power spectrum showing the main IF carrier frequencies and higher order mixing products. The boxes represent 100 kHz detection bandwidth for polarimetry carrier centered at ~ 730 kHz, and 200 kHz detection bandwidth for interferometry carriers centered at ~ 1170 and 1900 kHz. The smaller peaks are from mixing between the main IF carriers.

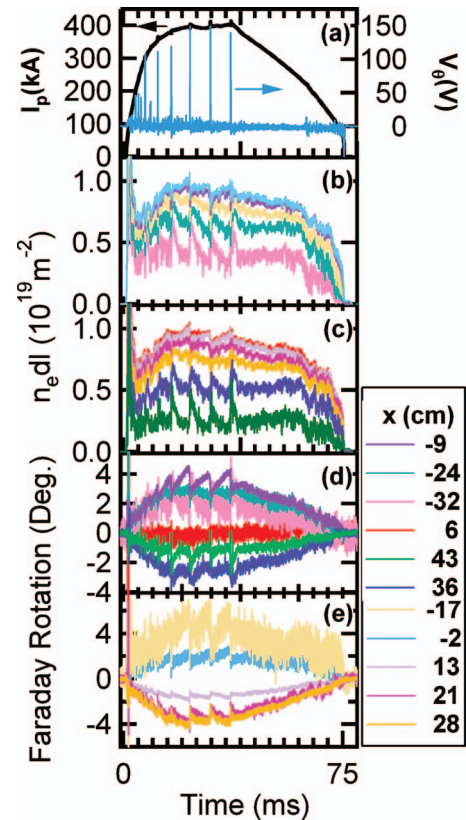


FIG. 3. (Color) Time traces from a single 400 kA standard plasma discharge, including plasma current and poloidal voltage (a); simultaneously measured line-integrated electron density [(b) and (c)] and Faraday rotation [(d) and (e)] from the 11 chords, indicated by their impact parameters x . The spikes in V_θ indicate sawtooth crashes. Data have 50 kHz bandwidth and are plotted every $10 \mu\text{s}$. Equilibrium profiles from this shot are shown in Figs. 4 and 5.

parametrized fitting method⁷ is used to obtain the toroidal current profiles and poloidal magnetic field profiles, using a fitting function shown below:

$$J_{\text{tor}} = J_0 \left(1 + \sum_{i=1, N} c_i r^{2i} \right) \exp(-r^2/w^2), \quad (1)$$

where c_i and w are coefficients defining the profile shape and J_0 is the current density on the axis. These free parameters are optimized to fit the measured Faraday rotation profile, constrained by the total plasma current. This function can fit centrally peaked, flat, or hollow current profiles and allows for reversed current near the edge. Profiles obtained with $N=3$ or 4 essentially have no difference within error bars.

Previously, polarimetry measurements of current profile evolution during sawtooth oscillations were achieved by ensemble averaging the data over a number of similar shots.^{1,2,7,8} With the three-wave polarimeter-interferometer, the current profile evolution can be measured in a single discharge for a single event. In Fig. 4, profiles before (22.6 ms), during (22.7 ms), and after (22.8 ms) a sawtooth crash are shown, using the data provided in Fig. 3. In Fig. 4(a), measured Faraday rotation angles are shown as discrete points and the smooth curves represent the results of the fitting analysis. Error bars indicate the standard deviation of the measured Faraday rotation angles and are mostly due to magnetic and density fluctuations. The relative error of the

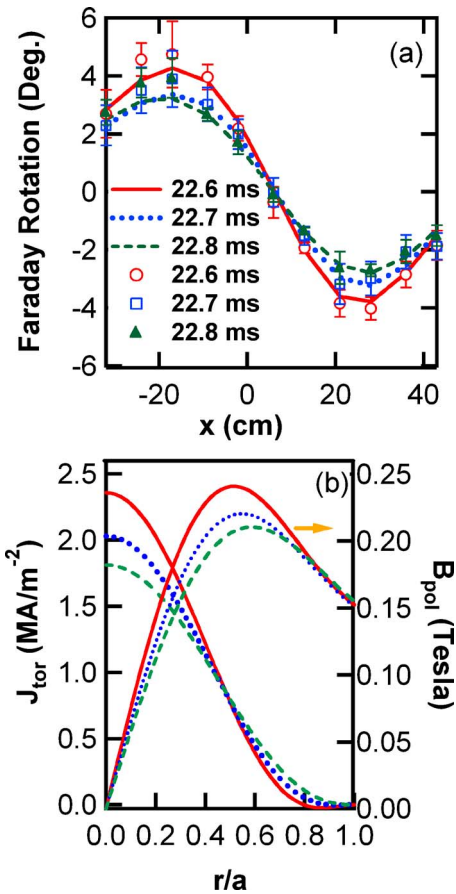


FIG. 4. (Color online) Equilibrium profiles of Faraday rotation (a), current density, and poloidal magnetic field (b) before (22.6 ms), during (22.7 ms), and after (22.8 ms) a single sawtooth crash event. Symbols represent the measurement points and curves are a best fit.

fitted current and magnetic profiles at the crash is 10%. In between sawtooth crashes, the relative error is below 5%. As expected, the current and magnetic field [Fig. 4(b)] profiles flatten during the sawtooth crash. Current density on the axis J_0 drops $\sim 30\%$ in 100–200 μs .

Equilibrium current density, poloidal magnetic field, and electron density profile evolution during the period of 10–40 ms are shown in Fig. 5. Time resolution is chosen to be 0.1 ms. For single-shot, single-event analysis, evaluating equilibrium profiles with higher time response is problematic since the effect of magnetic and density fluctuations is significant. Smaller time slices can be used if the data are first ensemble averaged over many events to remove the effects of fluctuations. Peaking of the J_{tor} profile during the slow linear ramp phase of the sawtooth cycle and fast flattening at the crash are clearly resolved. The decrease of B_{pol} in the plasma core at sawtooth crashes results from the reduction of core current. The total plasma current usually changes by less than 2% at a sawtooth crash, making the change in B_{pol} near the plasma edge small. During the linear ramp phase of a sawtooth cycle, n_e profiles in the core ($r < \sim 25$ cm) are slightly hollow and flattened about 2 ms before sawtooth crash, quite different from centrally peaked J_{tor} profile evolution. At sawtooth crashes, n_e profiles are flattened over the minor cross section. Differences between individual sawtooth cycles are clearly observed. This is especially true

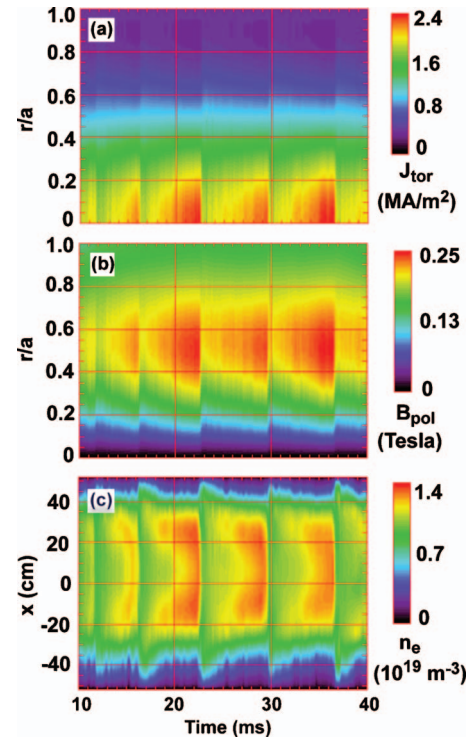


FIG. 5. (Color) Contour plots of (a) toroidal current, (b) poloidal magnetic field, and (c) electron density profile evolution in MST. At sawtooth crashes, J_{tor} on the axis collapses from ~ 2.5 to about 1.8 MA/m².

when comparing sawtooth cycles during the early current rise phase ($t < 20$ ms) and the current flat top phase ($20 < t < 40$ ms). This illustrates the advantage of having simultaneous Faraday rotation and interferometer measurements using the three-wave polarimeter-interferometer diagnostic.

For pellet injection⁹ experiments, pellet velocity and firing time as well as the dynamic plasma response vary significantly from shot to shot. Simultaneous measurement capability of the three-wave polarimeter-interferometer is critical for accurately diagnosing these plasmas. Shown in Figs. 6(a)–6(c) are the measured Faraday rotation profiles before (17 ms), during (19 ms), and after (22 ms) pellet in-

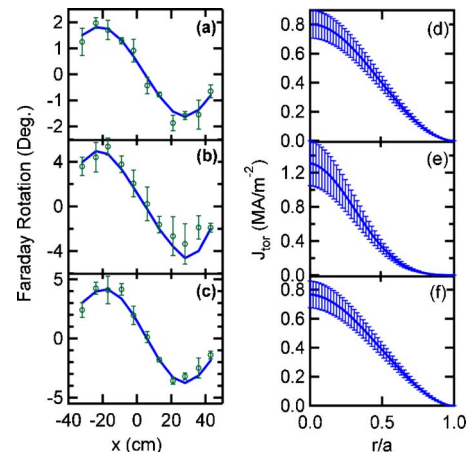


FIG. 6. (Color online) (a)–(c) Measured Faraday rotation and (d)–(f) fitted toroidal current profiles for a 200 kA standard discharge before (top), during (middle), and after (bottom) pellet injection. The solid curves in (a)–(c) result from profile analysis and represent a best fit to the data.

jection for a standard 200 kA plasma discharge. The open circles are the measurement points averaged over 0.2 ms, and the error bars represent the standard deviation. During pellet injection, the plasma central density changes from $1 \times 10^{19} \text{ m}^{-3}$ at 17 ms to $1.5 \times 10^{19} \text{ m}^{-3}$ at 19 ms, and $4 \times 10^{19} \text{ m}^{-3}$ at 22 ms. The corresponding J_{tor} profiles, shown in Figs. 6(d)–6(f), represent the first ever measurement of current profile evolution during pellet injection. These data clearly demonstrate the outstanding performance of the three-wave polarimeter-interferometer diagnostic on MST and its capability to study fast dynamic behavior of high-temperature plasmas.

In summary, a three-wave FIR laser polarimeter-interferometer system has been successfully developed for the MST reversed field pinch and is being routinely utilized in various experiments. The capability to simultaneously measure plasma current and magnetic profile dynamics in a single discharge with high time resolution has been demonstrated and shown to be necessary for experiments such as pellet injection or sawtooth dynamics, where the plasma re-

sponse can vary significantly from shot to shot or event to event. By including additional information from external coils on the average and edge values of the toroidal magnetic field, it is possible to expand our analysis to include determination of the toroidal field, safety factor, and plasma pressure profiles. This work is ongoing and will be presented separately.

ACKNOWLEDGMENT

This work is supported by U.S. Department of Energy.

- ¹D. L. Brower *et al.*, Phys. Rev. Lett. **88**, 185005 (2002).
- ²D. L. Brower *et al.*, Rev. Sci. Instrum. **74**, 1534 (2003).
- ³W. X. Ding *et al.*, Phys. Rev. Lett. **93**, 045002 (2004).
- ⁴J. H. Rommers and J. Howard, Plasma Phys. Controlled Fusion **38**, 1805 (1996).
- ⁵Y. Jiang, D. L. Brower, L. Zeng, and J. Howard, Rev. Sci. Instrum. **68**, 902 (1997).
- ⁶N. E. Lanier *et al.*, Phys. Plasmas **8**, 3402 (2001).
- ⁷S. D. Terry *et al.*, Phys. Plasmas **11**, 1079 (2004).
- ⁸H. Soltwisch and H. R. Koslowski, Plasma Phys. Controlled Fusion **37**, 667 (1995).
- ⁹S. K. Combs *et al.*, Fusion Sci. Technol. **44**, 513 (2003).